

# On the validity of the adiabatic approximation in compact binary inspirals

Andrea Maselli,<sup>1</sup> Leonardo Gualtieri,<sup>1</sup> Francesco Pannarale,<sup>2</sup> and Valeria Ferrari<sup>1</sup>

<sup>1</sup>*Dipartimento di Fisica, “Sapienza” Università di Roma & Sezione INFN Roma1, Rome, Italy*

<sup>2</sup>*Max-Planck-Institut für Gravitationsphysik, Albert Einstein Institut, Potsdam, Germany*

Using a semi-analytical approach recently developed to model the tidal deformations of neutron stars in inspiralling compact binaries, we study the dynamical evolution of the tidal tensor, which we explicitly derive at second post-Newtonian order, and of the quadrupole tensor. Since we do not assume *a priori* that the quadrupole tensor is proportional to the tidal tensor, i.e. the so called “adiabatic approximation”, our approach enables us to establish to which extent such approximation is reliable. We find that the ratio between the quadrupole and tidal tensors (i.e., the Love number) increases as the inspiral progresses, but this phenomenon only marginally affects the emitted gravitational waveform. We estimate the frequency range in which the tidal component of the gravitational signal is well described using the stationary phase approximation at next-to-leading post-Newtonian order, comparing different contributions to the tidal phase. We also derive a semi-analytical expression for the Love number, which reproduces within a few percentage points the results obtained so far by numerical integrations of the relativistic equations of stellar perturbations.

PACS numbers: 04.30.-w, 04.25.Nx, 04.25.dk

## I. INTRODUCTION

Coalescing binary systems of neutron stars (NS) and/or black holes (BH) are among the most interesting sources of gravitational waves (GWs) to be detected by advanced Virgo and LIGO [1]. One of the key features of the coalescence is the NS tidal deformation, which provides precious information on the NS equation of state (EOS) [2–6]. For this reason, theoretical and numerical studies have been recently performed to model the effect of tidal deformations on the emitted GW signal, and to extract its contribution from a detected signal [2, 3, 5–11]. These studies are based on fully general-relativistic numerical simulations and on (semi-)analytical approaches.

In current analytical approaches, the tidal deformation properties of NSs are encoded in a set of numbers, the *Love numbers* [2–6, 12, 13], which relate the mass multipole moments of the star to the (external) tidal field multipole moments. In the so-called “adiabatic approximation”, at the lowest multipole order, the evolution of a star in response to an external quadrupolar tidal field  $C_{ij}$ , is governed by the equation

$$Q_{ij} = -\frac{2}{3}k_2 R_{\text{NS}}^5 C_{ij}, \quad (1)$$

where  $Q_{ij}$  is the star quadrupole moment,  $R_{\text{NS}}$  is its radius at isolation, and  $k_2$  is the (dimensionless)  $l = 2$  apsidal constant, also dubbed *second tidal Love number*. For non-rotating relativistic stars,  $k_2$  is usually computed by solving the linear  $l = 2$  static, even-parity perturbations of Tolman-Oppenheimer-Volkoff solutions [14], requiring regularity and continuity for the metric perturbation and its first derivative [4, 12, 13]. Eq. (1) and its higher multipole order versions have been employed to determine the effect of tidal deformations on the orbital motion, and on the GW signal emitted by NS-NS and BH-NS binary systems [3, 5, 6, 9]. In these studies, the relation in

Eq. (1) — or an equivalent assumption [5] — is assumed as a starting point.

The domain of validity of (1) is briefly discussed in [2], using previous results of Lai. In [15] a NS tidally interacting with a companion, is described as a forced oscillator in a Newtonian framework; the energy absorbed by the oscillator is the sum of an “instantaneous” term, proportional to the forcing (tidal) field, and a term associated with the stellar oscillations. Since the former is much larger than the latter, it is argued that the adiabatic approximation (1) holds [2]. A forced oscillator model is also used in [3], providing further evidence of the accuracy of the adiabatic approximation. It should be stressed, however, that only a consistent dynamical study of the stellar deformation during the inspiral may assess the validity of the adiabatic approximation. This is the approach we follow in this paper.

In a recent work [16], some of us developed a semi-analytical description of tidal deformations of NSs in inspiralling BH-NS and NS-NS binaries. This model combines the post-Newtonian (PN) approach (see, for instance, [17–19]), which accurately describes the orbital motion before the onset of mass-shedding, and the *affine model*, which allows for a description of stellar deformations due to an external quadrupolar tidal field generated by the companion [20–25]. We computed the tidal tensor associated with the PN metric of a two-body system, defined in terms of the PN Riemann tensor and of the NS local tetrad

$$C_{ij} = R_{\alpha\beta\gamma\delta} e_{(0)}^\alpha e_{(i)}^\beta e_{(0)}^\gamma e_{(j)}^\delta, \quad (2)$$

up to 1.5PN order. This tensor appears as a source in the dynamical equations describing the stellar deformations. Note that the use of a two-body PN metric explicitly yields self-interaction terms in the tidal tensor. We validated our post-Newtonian-affine (PNA) approach by comparing the results obtained for BH-NS binaries to the outcome of fully general-relativistic numerical simu-

lations. In addition, we computed the Love number  $k_2$  using Eq. (1) at large separations, showing that our results were in good agreement with the analytical results of [12].

In this paper, we extend the PNA approach further:

- We compute the tidal tensor (2) up to 2PN order. This new result may allow one to construct more accurate models of gravitational waveforms emitted by inspiralling compact binaries, which could be employed to extract information on the Love number and on the underlying equation of state, during post-processing. Indeed, the 2PN terms may be used to correct the binary binding energy and the GW-flux and to improve the description of the phase evolution.
- We use the 2PN tidal tensor to assess the range of validity of the adiabatic approximation. We do so by solving the dynamical equations for the orbital motion and the stellar deformations, by computing the quadrupole and tidal tensors, and by determining  $k_2$  from

$$k_2 = -\frac{3Q_{ij}}{2R_{\text{NS}}^5 C_{ij}}, \quad (3)$$

at different values of the orbital separation. We find that  $k_2$  increases in the late inspiral phase; it should thus be referred to as a *Love function*  $k_2(r)$ , of which  $k_2$  is the asymptotic limit. As discussed in Section III, we prefer to express  $k_2$  as a function of  $r$ , rather than as a function of the gauge invariant frequency, because in this way it is easier to find an accurate fit for  $k_2$ . We then use the stationary phase approximation [26, 27] to compute the gravitational waveforms with tidal phase effects included up to 1PN relative order [9] and model the gravitational wave phase accordingly.

- We compute the fitting factors [28] between point-particle templates and a model of the gravitational signal that includes tidal effects at the best of our knowledge up to 1PN order, i.e., including the Love function  $k_2(r)$ . We find that point particle templates satisfy the accuracy standards defined in [28], unless one considers NS-NS binaries with a very stiff equation of state, in which case the aforementioned standards are marginally violated. Moreover, we show that tidal effects can affect the measurement of the total mass and the symmetric mass ratio by at most 3% and 2%, respectively.
- We derive a simple, semi-analytical expression for the tidal Love number  $k_2$ :

$$k_2 = \frac{15}{4} \frac{\hat{\mathcal{M}}^2}{\hat{\Pi} R_{\text{NS}}^5},$$

where  $\hat{\mathcal{M}}$  and  $\hat{\Pi}$  are, respectively, the scalar quadrupole moment of the star and the integral

of the pressure over the stellar volume, both calculated for the star at isolation. We check the accuracy of this formula by comparing its results to those obtained by perturbative approaches [12], finding that they agree within a few percentage points.

The plan of the paper is the following. In Sec II we briefly describe our model. In Sec. III we study the tidal Love number  $k_2$  in the post-Newtonian affine approach. In Sec. IV we compute the gravitational waveform in the stationary phase approximation, comparing the different tidal contributions to the Fourier phase. In Sec. V we compare the waveforms obtained by using different approximations for the tidal contributions to the Fourier phase. In Sec. VI we draw the conclusions.

## II. THE MODEL

In the following we briefly sketch the post-Newtonian-affine model. For further details, see [16]. The masses of the two compact objects, inspiralling on quasi-circular orbits, are  $m_1$  and  $m_2$ ,  $m = m_1 + m_2$  is the total mass, and  $\nu = m_1 m_2 / m^2$  is the symmetric mass ratio. We write the equations for the secondary object  $m_2$ , of radius  $R_{\text{NS}}$ . In a NS-NS system, analogous equations hold for the primary object  $m_1$ .

### A. Tidal deformations in the affine model

To describe the stellar deformation, we use the affine model approach [20–22] (improved in [16, 24, 25]), which is based on the assumption that a NS in a binary system preserves an ellipsoidal shape when it is deformed by the tidal field of the companion. The deformation equations are written in the principal frame, i.e., the one comoving with the star and with axes coincident with the principal axes of the ellipsoid. Surfaces of constant density inside the star form self-similar ellipsoids, and the velocity of a fluid element is a linear function of the coordinates  $x^i$  of the principal frame. Under these assumptions, the infinite degrees of freedom of the stellar fluid reduce to five dynamical variables and we are left with a set of ordinary differential equations describing the evolution of the star. The five variables describing the stellar deformation are the three principal axes of the ellipsoid<sup>1</sup>  $a_i$  ( $i = 1, 2, 3$ ) and two angles  $\psi, \lambda$  defined as

$$\frac{d\psi}{d\tau} = \Omega, \quad \frac{d\lambda}{d\tau} = \Lambda, \quad (4)$$

<sup>1</sup> In our conventions, '1' denotes the direction along the axis directed towards the companion, '2' is the direction along the other axis that lies in the orbital plane, and '3' indicates the direction of the axis orthogonal to the orbital plane.

where  $\tau$  is the NS proper time,  $\Omega$  is the ellipsoid angular velocity measured in the parallel transported frame associated with the star center of mass (the “figure” velocity in [22]), and  $\Lambda$  (defined in [22] in terms of the vorticity along the  $z$ -axis in the corotating frame) describes the internal fluid motion in the principal frame.

The NS internal dynamics is described in terms of the Lagrangian

$$\mathcal{L}_I = T_I - U - \mathcal{V} \quad (5)$$

where  $T_I$  is the star kinetic energy,  $U$  is the internal energy of the stellar fluid, and  $\mathcal{V}$  is the star self-gravity. The relevant integrals are the scalar quadrupole moment  $\mathcal{M} = 1/3 \int dM_B \sum_i (x_i)^2$ , the pressure integral  $\Pi = \int dM_B p/\rho$ , and the self-gravity potential  $\mathcal{V} = -\int dM_B \sum_i x_i \partial_i \Phi$ ; here  $dM_B$  is the baryon mass element,  $\Phi$  is the gravitational potential,  $p$  is the pressure, and  $\rho$  is the baryon mass density.

As shown in [20, 21], under the affine hypothesis the integrals  $\mathcal{M}$ ,  $\Pi$ ,  $\mathcal{V}$  can be expressed in terms of integrals over the spherical configuration of the star ( $a_i = R_{\text{NS}}$ ), and of functions of the dynamical variables. In the following, all carets ( $\hat{\phantom{x}}$ ) denote quantities computed on the spherical star. In the spherical configuration, the pressure integral and the self-gravity are related by the virial theorem

$$\hat{\mathcal{V}} = -3\hat{\Pi}. \quad (6)$$

The original affine approach, introduced in a Newtonian framework [20–22], was improved and extended in [16, 24, 25]. The spherical configuration of the star is determined by solving the relativistic equations of stellar structure, which yield the profile of  $\hat{p}(r_s)$ , being  $r_s$  the radial coordinate in a Schwarzschild frame associated to the NS. The gravitational potential  $\Phi$  appearing in the definition of  $\mathcal{V}$  is replaced by an effective relativistic potential such that the virial theorem (6) is satisfied. The equations of motion for the internal variables  $q_i = \{\psi, \lambda, a_1, a_2, a_3\}$  and their conjugate momenta  $p_i = \{p_\psi, p_\lambda, p_{a_1}, p_{a_2}, p_{a_3}\}$  are:

$$\frac{da_1}{dt} = \frac{R_{\text{NS}}}{\gamma(t)} \frac{p_{a_1}}{\hat{\mathcal{M}}} \quad (7)$$

$$\frac{da_2}{dt} = \frac{R_{\text{NS}}}{\gamma(t)} \frac{p_{a_2}}{\hat{\mathcal{M}}} \quad (8)$$

$$\frac{da_3}{dt} = \frac{R_{\text{NS}}}{\gamma(t)} \frac{p_{a_3}}{\hat{\mathcal{M}}} \quad (9)$$

$$\frac{dp_{a_1}}{dt} = \frac{\hat{\mathcal{M}}}{\gamma(t)} \left[ \Lambda^2 + \Omega^2 - 2\frac{a_2}{a_1}\Lambda\Omega + \frac{1}{2}\frac{\hat{\mathcal{V}}}{\hat{\mathcal{M}}} R_{\text{NS}}^3 \tilde{A}_1 + \frac{R_{\text{NS}}^2}{\hat{\mathcal{M}}} \frac{\Pi}{a_1^2} - c_{xx} \right] a_1 \quad (10)$$

$$\frac{dp_{a_2}}{dt} = \frac{\hat{\mathcal{M}}}{\gamma(t)} \left[ \Lambda^2 + \Omega^2 - 2\frac{a_1}{a_2}\Lambda\Omega + \frac{1}{2}\frac{\hat{\mathcal{V}}}{\hat{\mathcal{M}}} R_{\text{NS}}^3 \tilde{A}_2 + \frac{R_{\text{NS}}^2}{\hat{\mathcal{M}}} \frac{\Pi}{a_2^2} - c_{yy} \right] a_2 \quad (11)$$

$$\frac{dp_{a_3}}{dt} = \frac{\hat{\mathcal{M}}}{\gamma(t)} \left[ \frac{1}{2}\frac{\hat{\mathcal{V}}}{\hat{\mathcal{M}}} R_{\text{NS}}^3 \tilde{A}_3 + \frac{R_{\text{NS}}^2}{\hat{\mathcal{M}}} \frac{\Pi}{a_3^2} - c_{zz} \right] a_3 \quad (12)$$

$$\frac{d\lambda}{dt} = \frac{\Lambda}{\gamma(t)} \quad (13)$$

$$\frac{dp_\lambda}{dt} = \frac{\dot{\mathcal{C}}}{\gamma(t)} = 0 \quad (14)$$

$$\frac{d\psi}{dt} = \frac{\Omega}{\gamma(t)} \quad (15)$$

$$\frac{dp_\psi}{dt} = \frac{\dot{J}_2}{\gamma(t)} = \frac{\hat{\mathcal{M}}}{R_{\text{NS}}} \frac{c_{xy}}{\gamma(t)} (a_2^2 - a_1^2). \quad (16)$$

In the above equations, the  $c_{ij}$ ’s are the PN tidal tensor components defined later in Sec. II C,

$$\tilde{A}_i \equiv \int_0^\infty \frac{du}{(a_i^2 + u)\sqrt{(a_1^2 + u)(a_2^2 + u)(a_3^2 + u)}} \quad (17)$$

are elliptic integrals,

$$\gamma(t) = 1 + \frac{\chi_1}{c^2} \left( \frac{Gm}{r} + \frac{v^2}{2}\chi_1 \right) + \frac{\chi_1}{2c^4} \left\{ \frac{G^2 m^2}{r^2} [1 - 4\chi_2] + \frac{Gm}{r} v^2 [5 - \chi_2(1 + 2\chi_1\chi_2)] + \chi_1 \left[ 1 - 3\chi_1 + \frac{11}{4}\chi_1^4 \right] v^4 \right\} \quad (18)$$

$$\hat{\mathcal{M}} = \frac{4\pi}{3} \int_0^{R_{\text{NS}}} \hat{\rho} \left( 1 - \frac{2V(r_s)}{c^2} + \frac{Gm(r_s)}{r_s c^2} \right) r_s^4 dr_s \quad (19)$$

$$\Pi = \frac{a_1 a_2 a_3}{R_{\text{NS}}^3} 4\pi \int_0^{R_{\text{NS}}} \hat{p} \left( \hat{\rho} \frac{R_{\text{NS}}^3}{a_1 a_2 a_3} \right) \left( 1 + \frac{Gm(r_s)}{r_s c^2} \right) r_s^2 dr_s \quad (20)$$

where  $\chi_A = m_A/m$  ( $A = 1, 2$ ),  $V(r_s) \equiv G \int_{r_s}^\infty \frac{m_s(r'_s)}{r_s'^2} dr'_s$ ,  $m_s(r_s)$  is the gravitational mass enclosed in a sphere of radius  $r_s$ ,  $r$  and  $v$  are the orbital distance and the relative velocity of the two bodies in the PN frame, and

$$\mathcal{C} = \frac{\hat{\mathcal{M}}}{R_{\text{NS}}^2} [(a_1^2 + a_2^2)\Lambda - 2a_1 a_2 \Omega], \quad J_2 = \frac{\hat{\mathcal{M}}}{R_{\text{NS}}^2} [(a_1^2 + a_2^2)\Omega - 2a_1 a_2 \Lambda] \quad (21)$$

are the circulation and the NS spin angular momentum. In this article we consider the case of an asymptotically

non-rotating star. As discussed in [22], the intrinsic spin of the star may be defined only far away from the companion, where the star is axisymmetric and the ellipsoid rotation  $\Omega$  vanishes; in this region, it is possible to identify the angular velocity of the star with  $-\Lambda$ . Therefore, an asymptotically non-rotating star has  $\Lambda = 0$ ,  $\Omega = 0$ , and thus  $\mathcal{C} = 0$ , at  $r \rightarrow \infty$ . Since  $\mathcal{C}$  is a constant of motion, it remains zero during the inspiral.  $\Omega$  and  $\Lambda$ , instead, become non-vanishing as the NS couples with the tidal field, i.e., the ellipsoidal star acquires a (very small) angular velocity associated with general relativistic effects, such as geodetic precession and frame dragging.

## B. The orbital motion

The orbital motion is described in the post-Newtonian framework starting from the the 3PN metric of the two-body system, written in harmonic coordinates  $\{x^0 = ct, x, y, z\}$  [30, 31]. We assume an adiabatic inspiral of quasi-circular orbits, i.e. such that the energy carried out by GWs is balanced by the change of the total binding energy of the system [18]. We use the Taylor T4 approximant to describe the orbital phase evolution of the two-body system, including the effects of the tidal interaction on the orbital motion, derived at the 1PN order (beyond the leading term) in [9]. The phase  $\phi(t)$  and the orbital frequency  $\omega = d\phi(t)/dt$  are found by numerically integrating the following ordinary differential equations:

$$\frac{dx}{dt} = \mathcal{F}_{\text{pp}} + \mathcal{F}_{\text{tid}} \quad (22)$$

$$\frac{d\phi}{dt} = \frac{c^3}{Gm} x^{3/2} \quad (23)$$

where

$$x = \left( \frac{Gm\omega}{c^3} \right)^{2/3}, \quad (24)$$

$\mathcal{F}_{\text{pp}}$  is the point-particle term [32], and  $\mathcal{F}_{\text{tid}}$  incorporates the finite-size effects on the orbital motion [9]. To de-

termine the radial coordinate  $r(t)$ , we employ the PN expression for  $\gamma = \frac{Gm}{rc^2}$  (not to be confused with the time dilation factor  $\gamma(t)$  defined in Eq. (18)), which is also known up to 3PN order [33]. We refer to [16] for the explicit form of the equations, or to the original papers [18, 33].

## C. The post-Newtonian tidal tensor

The quadrupolar tidal tensor is

$$C_{ij} = R_{\alpha\beta\gamma\delta} e_{(0)}^\alpha e_{(i)}^\beta e_{(0)}^\gamma e_{(j)}^\delta, \quad (25)$$

where  $R_{\alpha\beta\gamma\delta}$  is the Riemann tensor of the 3PN metric describing the orbital motion. We introduce an orthonormal tetrad field  $e_{(i)}$  ( $i = 0, \dots, 3$ ) associated with the frame fixed to the star center of mass  $\mathcal{O}^*$ , parallel transported along its motion, and such that  $e_{(0)}^\mu = u^\mu$ , i.e., the 4-velocity of  $\mathcal{O}^*$ . In [16] we computed  $C_{ij}$  up to  $\mathcal{O}(1/c^3)$ , whereas previous computations were performed up to  $\mathcal{O}(1/c^2)$  [34, 35]. In this work we further expand the PN tidal tensor in order to include also  $1/c^4$  terms. To this aim we first need to calculate the 2PN component of the spatial tetrad vectors  $e_{(k)}^j$  introduced in [36]. From the orthogonality condition  $g_{\mu\nu} e_{(i)}^\mu e_{(j)}^\nu = \delta_{ij}$  we find that the tetrad field expanded up to  $1/c^4$  order for the bodies  $A = 1, 2$  is:

$$\begin{aligned} e_{(t)A}^t &= \tilde{e}_{(t)A}^t \\ e_{(t)A}^j &= \tilde{e}_{(t)A}^j \\ e_{(j)A}^t &= \tilde{e}_{(j)A}^t \\ e_{(x)A}^j &= \tilde{e}_{(x)A}^j \cos \xi_A + \tilde{e}_{(y)A}^j \sin \xi_A \\ e_{(y)A}^j &= -\tilde{e}_{(x)A}^j \sin \xi_A + \tilde{e}_{(y)A}^j \cos \xi_A \\ e_{(z)A}^j &= \tilde{e}_{(z)A}^j \end{aligned}$$

with

$$\begin{aligned} \tilde{e}_{(t)A}^t &= 1 + \frac{1}{c^2} \left[ (V)_A + \frac{v_A^2}{2} \right] + \frac{1}{c^4} \left[ \frac{5}{2} v_A^2 (V)_A + \frac{1}{2} (V^2)_A + \frac{3}{8} v_A^4 - 4v_A^i (V_i)_A \right] + \mathcal{O}(c^{-6}) \\ \tilde{e}_{(t)A}^j &= \frac{v_A^j}{c} + \left[ (V)_A + \frac{v_A^2}{2} \right] \frac{v_A^j}{c^3} + \mathcal{O}(c^{-5}) \\ \tilde{e}_{(j)A}^t &= \frac{v_A^j}{c} + \frac{1}{c^3} \left[ -4(V_j)_A + v_A^j \left( 3(V)_A + \frac{v_A^2}{2} \right) \right] + \mathcal{O}(c^{-5}) \\ \tilde{e}_{(k)A}^j &= \delta_k^j \left[ 1 - \frac{(V)_A}{c^2} \right] + \frac{v_A^j v_A^k}{2c^2} + \frac{1}{8c^4} \left[ 4(V)_A^2 \delta_k^j + 3v_A^j v_A^k (4(V)_A + v_A^2) - 16(\hat{W}_{jk})_A \right] + \mathcal{O}(c^{-6}), \end{aligned} \quad (26)$$

where  $(V)_A$ ,  $(V_i)_A$ ,  $(\hat{W}_{ij})_A$  are PN potentials defined in terms of the source densities, evaluated at the location of

the body  $A$ , and regularized as described in [19]; finally,

$\xi_A$  is the angle describing geodesic precession and frame dragging

$$\xi_A = \frac{(\mathcal{Q}_{xy})_A}{c^2} \left[ 1 + \frac{1}{c^2} \left( (V)_A - \frac{v_A^2}{4} \right) \right]; \quad (27)$$

here  $\mathcal{Q}_{xy}$  is the non vanishing component of the antisymmetric matrix  $\mathcal{Q}$  defined as [36]:

$$\mathcal{Q}(t, t_0) = \int_{t_0}^t [\mathbf{v} \times (\nabla V - \mathbf{a}) - \nabla \times (V\mathbf{v} - 2\mathbf{V})] dt, \quad (28)$$

with  $t_0$  arbitrary initial time.

Following the same procedure described in [16] we project the Riemann tensor on the tetrad field, to derive the tidal tensor which we express in the NS principal frame as  $c = TCT^T$ , where

$$T = \begin{pmatrix} \cos \psi & \sin \psi & 0 \\ -\sin \psi & \cos \psi & 0 \\ 0 & 0 & 1 \end{pmatrix} \quad (29)$$

and  $\psi$  has been defined in Section II A. We find that the tidal tensor components for the body 2, appearing on the right-hand-side of the dynamical equations (10)-(12), are:

$$\begin{aligned} c_{xx} = & -\frac{Gm\chi_1}{2r^3} \{1 + 3 \cos[2\psi_l]\} + \frac{Gm\chi_1}{4c^2r^3} \left\{ \frac{Gm}{r} (5 + \chi_1) (1 + 3 \cos[2\psi_l]) - 6v^2 (1 + \cos[2\psi_l]) \right\} + \frac{3G}{c^3} \frac{S_1^z \dot{\phi}}{r^3} \{\delta\chi + \\ & + (\chi_1 - 5\chi_2) \cos[2\psi_l]\} + \frac{Gm\chi_1}{c^4r^3} \left\{ \left[ \frac{G^2m^2}{r^2} \left( \frac{687}{28} \chi_2^2 - \frac{101}{8} \chi_2 - 9 \right) - \frac{Gm}{r} v^2 \left( 3\chi_2^2 + \frac{223}{16} \chi_2 + \frac{3}{2} \right) + \right. \right. \\ & \left. \left. - \frac{3}{2} v^4 (2\chi_2^2 - 2\chi_2 + 1) \right] \cos[2\psi_l] + \frac{G^2m^2}{r^2} \left( \frac{229}{28} \chi_2^2 + \frac{\chi_2}{8} - 3 \right) - \frac{Gm}{r} v^2 \left( \chi_2^2 + \frac{109}{16} \chi_2 + \frac{3}{2} \right) + \right. \\ & \left. \left. - \frac{3}{2} (2\chi_2^2 - 2\chi_2 + 1) v^4 \right\} + \mathcal{O}(c^{-5}), \end{aligned} \quad (30)$$

$$\begin{aligned} c_{yy} = & -\frac{Gm\chi_1}{2r^3} \{1 - 3 \cos[2\psi_l]\} + \frac{Gm\chi_1}{4c^2r^4} \left\{ \frac{Gm}{r} (5 + \chi_1) (1 - 3 \cos[2\psi_l]) - 6v^2 (1 - \cos[2\psi_l]) \right\} + \frac{3G}{c^3} \frac{S_1^z \dot{\phi}}{r^3} \{\delta\chi + \\ & - (\chi_1 - 5\chi_2) \cos[2\psi_l]\} + \frac{Gm\chi_1}{c^4r^3} \left\{ \left[ -\frac{G^2m^2}{r^2} \left( \frac{687}{28} \chi_2^2 - \frac{101}{8} \chi_2 - 9 \right) + \frac{Gm}{r} v^2 \left( 3\chi_2^2 + \frac{223}{16} \chi_2 + \frac{3}{2} \right) + \right. \right. \\ & \left. \left. + \frac{3}{2} (2\chi_2^2 + 2\chi_2 + 1) v^4 \right] \cos[2\psi_l] + \frac{G^2m^2}{r^2} \left( \frac{229}{28} \chi_2^2 + \frac{\chi_2}{8} - 3 \right) - \frac{Gm}{r} v^2 \left( \chi_2^2 + \frac{109}{16} \chi_2 + \frac{3}{2} \right) + \right. \\ & \left. \left. - \frac{3}{2} (2\chi_2^2 - 2\chi_2 + 1) v^4 \right\} + \mathcal{O}(c^{-5}), \end{aligned} \quad (31)$$

$$\begin{aligned} c_{zz} = & \frac{Gm\chi_1}{r^3} - \frac{Gm\chi_1}{2c^2r^3} \left[ \frac{Gm}{r} (5 + \chi_1) - 6v^2 \right] - \frac{6G}{c^3} \frac{\dot{\phi} S_1^z}{r^3} \delta\chi + \frac{Gm\chi_1}{c^4r^3} \left\{ \frac{G^2m^2}{r^2} \left[ -\frac{229}{14} \chi_2^2 + \frac{51}{4} \chi_2 + 6 \right] + \right. \\ & \left. + \frac{Gm}{r} v^2 \left[ 2\chi_2^2 + \frac{5}{8} \chi_2 + 3 \right] + 3 [2\chi_2^2 - 2\chi_2 + 1] v^4 \right\} + \mathcal{O}(c^{-5}), \end{aligned} \quad (32)$$

$$\begin{aligned} c_{xy} = & \frac{3Gm\chi_1}{2r^3} \sin[2\psi_l] - \frac{3Gm\chi_1}{4c^2r^3} \left[ \frac{Gm}{r} (5 + \chi_1) - 2v^2 \right] \sin[2\psi_l] + \frac{3G}{c^3} \frac{S_1^z \dot{\phi}}{r^3} (5\chi_2 - \chi_1) \sin[2\psi_l] + \frac{Gm\chi_1}{c^4r^3} \times \\ & \times \left\{ \frac{G^2m^2}{r^2} \left[ -\frac{687}{28} \chi_2^2 + \frac{101}{8} \chi_2 + 9 \right] + \frac{Gm}{r} v^2 \left[ 3\chi_2^2 + \frac{223}{16} \chi_2 + \frac{3}{2} \right] + \frac{3}{2} [2\chi_2^2 - 2\chi_2 + 1] v^4 \right\} \sin[2\psi_l] + \mathcal{O}(c^{-5}). \end{aligned} \quad (33)$$

In the above expressions,  $\delta\chi = \chi_1 - \chi_2$  and the *lag* angle  $\psi_l = \psi - \phi + \xi$  describes the misalignment between the  $a_1$  axis and the line between the two objects. The superscript dot identifies derivatives of the orbital variables  $\phi$  with respect to the coordinate time  $t$ . It should be noted that in the center-of-mass frame of the binary system, the tidal tensor is given by the same expressions (30)-(33), setting  $\psi_l = -\phi$ . We also stress that, by construction, the tidal tensor is traceless.

Finally, we remark that (for a star with zero circulation, i.e.,  $\mathcal{C} = 0$ ) the lag angle is very small, since it is only due to general relativistic effects such as geodetic precession and frame dragging; therefore,  $\psi_l \ll 1$ . Then, since at leading order  $c_{xy} \propto \sin[2\psi_l]$ , it follows that

$$c_{xy} \ll c_{xx}, c_{yy}, c_{zz}. \quad (34)$$

We have checked numerically that  $c_{xy}$  is always several orders of magnitude smaller than the others components

of the tidal tensor. We remark that, as noted in [37], the lag angle becomes non-negligible when viscosity is included in the model.

### III. TIDAL LOVE NUMBERS IN THE POST-NEWTONIAN-AFFINE APPROACH

NS tidal deformations can be described in terms of a set of parameters, the Love numbers, encoding the deformation properties of the star. The idea is that in presence of a weak, external tidal field, a spherical star is deformed, and its mass multipole moments are proportional to the multipole moments of the perturbing tidal field. In this paper, we focus on the Love number  $k_2$ , which is associated with the lowest order “electric” moment, i.e., the  $\ell = 2$ , or quadrupole, moment. This is the most relevant for the phenomenology of stellar deformations, to be considered when modelling gravitational waveforms. The mass quadrupole moment (traceless) tensor is proportional to the tidal field [2, 12]:

$$Q_{ij} = -\frac{2}{3}k_2 R_{\text{NS}}^5 C_{ij}. \quad (35)$$

In the NS principal frame, this equation reads

$$q_{ij} = -\frac{2}{3}k_2 R_{\text{NS}}^5 c_{ij}, \quad (36)$$

where  $q_{ij}$  is the quadrupole moment tensor projected onto this frame

$$\begin{aligned} q_{ij} &= \int dM_B \left( x^i x^j - \frac{1}{3} \delta^{ij} r^2 \right) d^3x \\ &= \frac{\hat{\mathcal{M}}}{R_{\text{NS}}^2} (a_i^2 - a^2) \delta^{ij} \end{aligned} \quad (37)$$

(no sum on  $i$ ),  $a^2 = (a_1^2 + a_2^2 + a_3^2)/3$ , and  $\hat{\mathcal{M}}$  is the scalar quadrupole moment for the spherical, isolated star configuration given in Eq. (19).

Eq. (36) is based on the adiabatic approximation, which assumes that the timescale of the orbital evolution (and thus of tidal tensor variations) is much larger than the timescale needed for the star to readjust into a stationary configuration. In the following we will drop this assumption and assess its validity.

#### A. Evolution of the tidal Love number during the inspiral

We solve Eqns. (7)-(16), (22), and (23), for a representative set of binary system configurations. We consider two equations of state, dubbed APR (which had been derived by Akmal, Pandharipande and Ravenhall [37]) and PS (which had been derived by Pandharipande and Smith [38]). These EOSs are expected to cover the range of possible EOS stiffness and NS deformability: the APR EOS describes soft NS matter and yields NS models with

high compactness  $\mathcal{C}$  (not to be confused with the circulation defined in Eq. 21) and small deformability  $\lambda$ , whereas the PS EOS describes stiff NS matter and gives stellar models with small compactness and large deformability (see for instance [6]). We consider two values of the secondary NS mass,  $m_2 = 1.2 M_\odot, 1.4 M_\odot$ , and three values of the mass ratio,  $q = m_1/m_2 = 1, 3, 5$ . In the  $q = 1$  cases, both bodies are NSs, with the same EOS, and we take into account the deformation of both of them. When  $q = 3, 5$  we assume that primary body is a BH.

For each of these binary models, we compute  $k_2$  from Eq. (36), using Eq. (37) for the left-hand side. We find that this quantity is a function of the orbital distance,  $k_2(r)$ , and that it increases during the stellar inspiral. We express  $k_2$  as a function of  $r$ , and not of the PN variable  $x$ , because it is easier to find an accurate fit for  $k_2$  in terms of the  $r$ -dependence rather than of the  $x$ -dependence. Further, we think that the variable  $r$  provides a more direct physical insight on the process. Hereafter, we denote the asymptotic limit of the function  $k_2(r)$ , i.e., the Love number, as

$$\bar{k}_2 = \lim_{r \rightarrow \infty} k_2(r).$$

We determine  $\bar{k}_2$  by fitting our data with the following expression:

$$k_2(r) = \bar{k}_2 \left( 1 + \alpha \frac{m}{r} + \beta \frac{m^2}{r^2} + \gamma \frac{m^3}{r^3} \right). \quad (38)$$

In Fig. 1 we plot the function  $k_2(r)$  for all the binary configurations we considered. The figure shows that in the last stages of the inspiral, before the mass-shedding sets in,  $k_2(r)$  grows by a factor of  $\sim 10\% - 30\%$ . This effect is strongly dependent on the EOS choice: it is larger/smaller for a stiffer/softer EOS as PS/APR, or, equivalently, for a less/more compact NS. The dependence of this effect on the mass ratio  $q$  is weaker; the Love number increases more for larger values of the mass ratio, unless the star reaches the innermost circular orbit (ICO) before the mass-shedding sets in. It seems that this effect is nearly insensitive to the NS mass. We show the curves in Fig. 1 as functions of  $r$ , and not of  $r/m$ , because we find that this choice makes the common asymptotic limit of the curves more evident.

#### B. Equations of tidal deformation in the perturbative regime

In the limit of small deformations

$$\delta a_i^2 \equiv a_i^2 - R_{\text{NS}}^2 \ll a^2, \quad (39)$$

it is possible to derive a semi-analytical, closed form for the Love number  $\bar{k}_2$ , expressed in terms of the NS scalar quadrupole moment and of the integral of the pressure over the stellar volume.

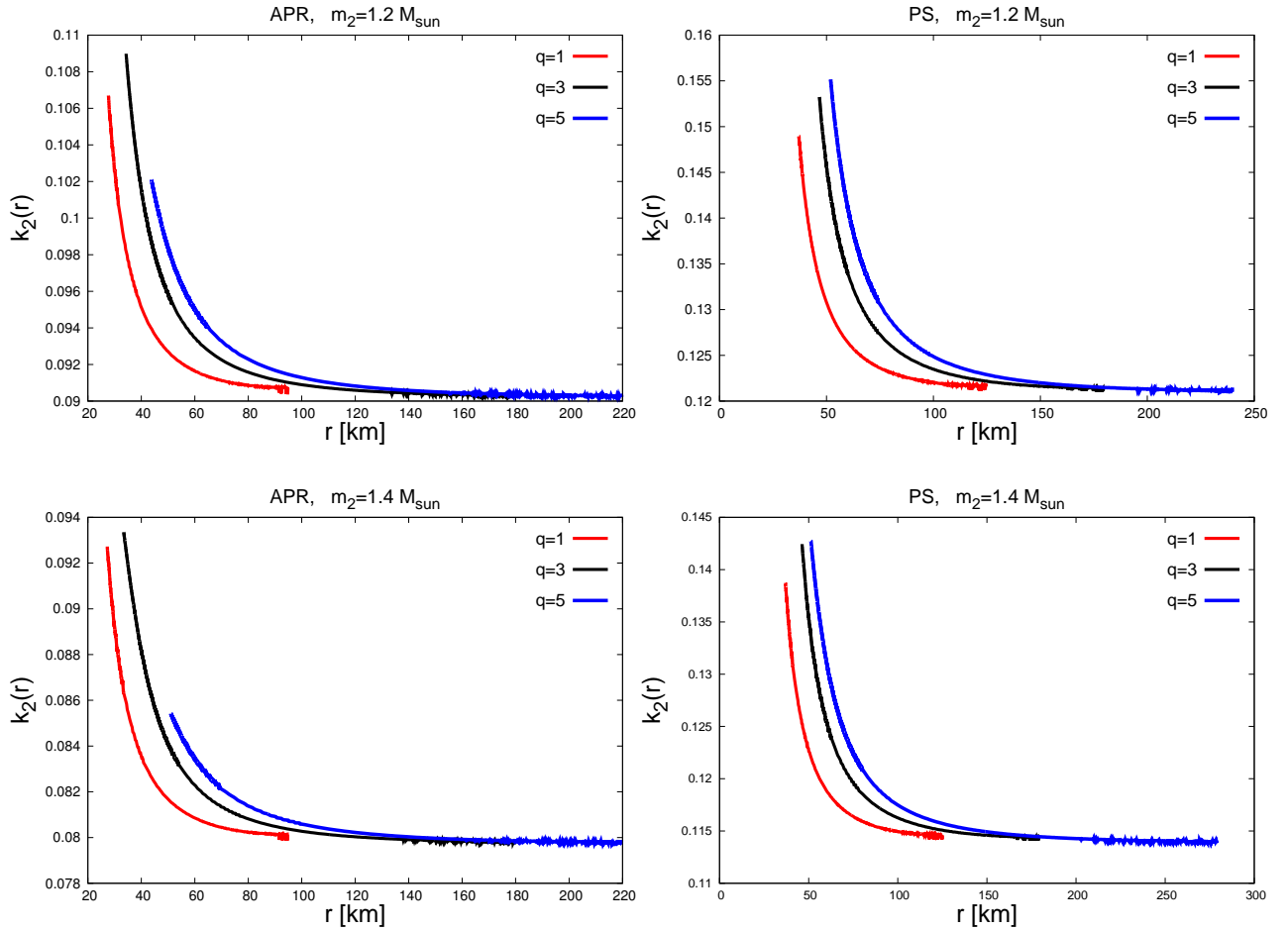


FIG. 1. (Color online) Love function  $k_2(r)$  for different choices of the NS EOS, NS mass  $m_2$ , and binary mass ratio  $q$ , as indicated in the panels. For the APR EOS,  $q = 5$ , and both values of the NS mass, the NS reaches the innermost circular orbit before the mass-shedding sets in.

By introducing the notation  $\delta a^2 \equiv \frac{1}{3} \sum_i \delta a_i^2 = a^2 - R_{\text{NS}}^2$ , we rewrite Eq. (37) as

$$q_{ij} = \frac{\hat{\mathcal{M}}}{R_{\text{NS}}^2} (\delta a_i^2 - \delta a^2) \delta^{ij} \quad (40)$$

(no sum on  $i$ ). As a first step, we show that the spherical, non rotating solution  $a_i = R_{\text{NS}}$ ,  $\Omega = \Lambda = 0$ , is a solution of Eqns. (7)-(16), with  $c_{ij} = 0$ . Indeed, in this limit the dynamical equations reduce to

$$\frac{\hat{\mathcal{M}}}{\gamma(t)} \left[ \frac{1}{2} \frac{\hat{\mathcal{V}}}{\hat{\mathcal{M}}} R_{\text{NS}}^3 \tilde{A} + \frac{\hat{\Pi}}{\hat{\mathcal{M}}} \right] = 0, \quad (41)$$

where we introduced  $\tilde{A} \equiv \tilde{A}_i(a_i = R_{\text{NS}})$ , which from Eq. (17) thus reads

$$\tilde{A} = \int_0^\infty \frac{du}{(R_{\text{NS}}^2 + u)^{5/2}} = \frac{2}{3} \frac{1}{R_{\text{NS}}^3}. \quad (42)$$

Eq. (41) is therefore satisfied when Eq. (6),  $\hat{\mathcal{V}} = -3\hat{\Pi}$ , i.e., the virial theorem, holds.

We now consider the first order perturbative expansion of Eqns. (7)-(16) around the spherical, non-rotating configuration. This expansion is an accurate description of the dynamical system when deformations are small, i.e., when the tidal field is weak and the rotation rate is small.

To simplify the discussion, we restrict the discussion to the case of an asymptotically non-rotating star; in this case Eq. (34) holds, i.e.,  $c_{xy} \ll c_{xx}, c_{yy}, c_{zz}$ , and Eqns. (13)-(16) and (21) guarantee that  $\Omega$ ,  $\Lambda$ ,  $\lambda$ , and  $\psi$  may be neglected. The remaining non-trivial equations, (10)-(12), reduce to

$$\frac{1}{2} \frac{\hat{\mathcal{V}}}{\hat{\mathcal{M}}} R_{\text{NS}}^3 \tilde{A}_i + \frac{R_{\text{NS}}^2}{\hat{\mathcal{M}}} \frac{\Pi}{a_i^2} - c_{ii} = 0 \quad (43)$$

( $i = 1, 2, 3$ , no sum on  $i$ ). We remark that in this proof the explicit expression of the tidal field  $c_{ij}$ , which drives the stellar deformation, can be taken as generic (we only require that  $c_{xy} \ll c_{xx}, c_{yy}, c_{zz}$ ).

Expanding Eq. (43) we find

$$\frac{\hat{\mathcal{V}}}{2\hat{\mathcal{M}}} \left( \frac{2}{3} - \frac{2}{5} \frac{\delta a_i^2}{R_{\text{NS}}^2} \right) + \frac{\hat{\Pi}}{\hat{\mathcal{M}}} \left( 1 + \frac{\delta \Pi}{\hat{\Pi}} - \frac{\delta a_i^2}{R_{\text{NS}}^2} \right) - c_{ii} = 0, \quad (44)$$

where we denoted the expansion of  $\Pi$  as  $\hat{\Pi} + \delta \Pi$  and considered the Taylor expansion of the integrals  $\tilde{A}_i$  (17) at first order in  $\delta a_i^2 = a_i^2 - R_{\text{NS}}^2$ , i.e.,

$$\tilde{A}_i = \frac{2}{3R_{\text{NS}}^3} - \frac{2}{5} \frac{\delta a_i^2}{R_{\text{NS}}^5}. \quad (45)$$

Imposing the virial theorem  $\mathcal{V} = -3\hat{\Pi}$ , one now has

$$\frac{\hat{\Pi}}{\hat{\mathcal{M}}} \left( \frac{\delta \Pi}{\hat{\Pi}} - \frac{2}{5} \frac{\delta a_i^2}{R_{\text{NS}}^2} \right) - c_{ii} = 0. \quad (46)$$

The traceless part of Eq. (46) yields

$$\frac{2}{5} \frac{\hat{\Pi}}{\hat{\mathcal{M}}} \frac{\delta a_i^2 - \delta a^2}{R_{\text{NS}}^2} = -c_{ii} \quad (47)$$

and plugging this into Eq. (40) gives

$$q_{ij} = \delta_{ij} \frac{\hat{\mathcal{M}}}{R_{\text{NS}}^2} (\delta a_i^2 - \delta a^2) = -\frac{5}{2} \frac{\hat{\mathcal{M}}^2}{\hat{\Pi}} c_{ij}. \quad (48)$$

A similar relation was found in [29].

Finally, Eqns. (36) and (48) yield the semi-analytical expression for the Love number we were looking for:

$$\bar{k}_2 = \frac{15}{4} \frac{\hat{\mathcal{M}}^2}{\hat{\Pi} R_{\text{NS}}^5}, \quad (49)$$

where  $\hat{\Pi}$  and  $\hat{\mathcal{M}}$  are given in Eqns. (20) and (19), respectively.

In Table I we show the quantities characterizing the different binary models considered in this paper, and the corresponding values of the Love number  $\bar{k}_2$ , computed in three different ways: (i) from the dynamical evolution of our equations (7)-(16), (22), (23); (ii) by solving the equations of relativistic stellar perturbations for an isolated NS, derived in [12] ( $\bar{k}_2^{\text{H}}$ ); (iii) from the semi-analytical formula (49) ( $\bar{k}_2^{\text{an}}$ ). We notice that, as expected (see also [16], where polytropic EOSs were considered), the less relativistic the NS is, i.e. the lower its compactness is, the lower the relative error between the relativistic value  $\bar{k}_2^{\text{H}}$  and our perturbative result  $\bar{k}_2^{\text{an}}$  is. Note that when the Love number is extracted from the dynamical evolution of the binary system, it has a (weak) dependence on the mass ratio  $q$ ; the quantities  $\bar{k}_2^{\text{H}}$ ,  $\bar{k}_2^{\text{an}}$ , instead, do not depend on  $q$ , because they are evaluated in terms of the intrinsic properties of the star. We find that the values of  $\bar{k}_2$  computed with these three approaches have very small discrepancies, of at most few percentage points.

Table I also provides the value of the orbital frequency  $f_{\text{cut}}^{\text{orb}}$  where our simulations stop. This corresponds to the onset of mass-shedding, or to the ICO, if the latter is encountered before mass-shedding (see discussion in [16]).

EOS	$m_2(M_\odot)$	$q$	$\bar{k}_2$	$\Delta \bar{k}_2 / \bar{k}_2$	$\Delta \bar{k}_2^{\text{an}} / \bar{k}_2$	$f_{\text{cut}}^{\text{orb}}(Hz)$
APR	1.2	1	0.0884	0.011	0.031	532.43
	1.2	3	0.089	0.019		500.32
	1.2	5	0.090	0.033		404.88 <sup>†</sup>
	1.4	1	0.079	0.047	0.058	575.88
	1.4	3	0.081	0.071		541.07
	1.4	5	0.080	0.063		347.07 <sup>†</sup>
PS	1.2	1	0.117	0.024	0.006	354.81
	1.2	3	0.114	0.048		332.39
	1.2	5	0.116	0.034		325.55
	1.4	1	0.110	0.017	0.017	378.04
	1.4	3	0.108	0.032		354.11
	1.4	5	0.112	0.005		345.20

TABLE I. Values of the Love number for different EOSs, NS masses  $m_2$ , and binary mass ratios  $q$  (columns 1,2,3, respectively). The value of  $\bar{k}_2$  given in column 4 is computed solving Eqns. (7)-(16), (22), and (23); in columns 5 and 6 we show the relative errors  $(\bar{k}_2 - \bar{k}_2^{\text{H}})/\bar{k}_2$  and  $(\bar{k}_2^{\text{an}} - \bar{k}_2^{\text{H}})/\bar{k}_2$ , where  $\bar{k}_2^{\text{H}}$  is the relativistic Love number computed solving the relativistic equations of stellar perturbations [12], and  $\bar{k}_2^{\text{an}}$  is evaluated using the semi-analytic formula (49) (see text). The values of the orbital frequency  $f_{\text{cut}}^{\text{orb}}$  at which our simulations end are also provided in the last column. The <sup>†</sup> symbol indicates that the ICO is reached before the onset of the mass-shedding.

#### IV. GRAVITATIONAL WAVEFORM IN THE POST-NEWTONIAN-AFFINE APPROACH

We now compute the gravitational waveform including tidal effects by means of the Love function  $k_2(r)$ . In the following derivation, we use geometric units  $G = c = 1$ . Our starting point is the state-of-the-art inclusion of tidal effects in the GW signal by means of the Love number  $\bar{k}_2$ . This is based on the binding energy  $\mathcal{E}(x)$  and the gravitational flux  $\mathcal{L}_{\text{GW}}(x)$  [9, 32]:

$$\mathcal{E}(x) = -\frac{m\nu x}{2} \left\{ \sum_{k=0}^6 e_k x^{k/2} - \bar{\lambda}_2 \frac{\chi_1}{\chi_2} \frac{x^5}{m^5} \times \right. \\ \left. \times \left[ 9 + \frac{11}{2} (3 + 2\chi_2 + 3\chi_2^2) x \right] + 1 \leftrightarrow 2 \right\}, \quad (50)$$

$$\mathcal{L}_{\text{GW}}(x) = \frac{32}{5} \nu^2 x^5 \left\{ \sum_{k=0}^7 f_k x^{k/2} + \frac{\bar{\lambda}_2}{\chi_2} \frac{x^5}{m^5} \times \right. \\ \left. \times \left[ 6(3 - 2\chi_2) - \frac{1}{28} (704 + 1803\chi_2 + \right. \right. \\ \left. \left. - 4501\chi_2^2 + 2170\chi_2^3) x \right] + 1 \leftrightarrow 2 \right\}, \quad (51)$$

where  $\bar{\lambda}_A$  ( $A = 1, 2$ ) is the tidal deformability associated with the  $A$ -th body and related to the Love number  $\bar{k}_{2,A}$  by

$$\bar{\lambda}_A = \frac{2}{3} \bar{k}_{2,A} R_{\text{NS}}^5. \quad (52)$$

The point-particle coefficients  $e_k, f_k$  are given in the Appendix of [32].

Using the stationary phase approximation (SPA) [26, 27] and the TaylorF2 framework [40] to construct the signal in the frequency domain, the  $(l, m_l)$  mode of the GW signal reads

$$\tilde{h}^{lm_l} \simeq \sqrt{\frac{2\pi}{m_l \ddot{\phi}(t_f)}} A^{lm_l} e^{i\psi^{lm_l}(f)}, \quad (53)$$

where  $t_f$  is defined as the time when the instantaneous frequency matches the Fourier variable, i.e.  $m_l \omega(t_f) = 2\pi f$ ,  $\phi$  is the orbital phase, the dots indicate a second derivative with respect to time,  $A^{lm_l}$  is the Fourier amplitude, and  $\psi^{lm_l} = 2\pi f t_f - m_l \phi(t_f) - \frac{\pi}{4}$  is the Fourier phase. To compute the  $\ddot{\phi} = \dot{\omega}$  entering the GW signal, we follow the strategy adopted in [32] and express  $\dot{\omega}$  as  $\dot{\omega} = \frac{3}{2m} \sqrt{\dot{x}\ddot{x}}$ , with  $\dot{x}$  derived using the TaylorT4 prescription given by Eq. (22). Hereafter, we shall focus on the  $l = m_l = 2$  mode of the gravitational waveform and drop the superscript “22” for sake of simplicity. The coefficients of the 3PN order expansion of the amplitude  $A(x)$  are collected in [32]. The Fourier phase has the form

$$\psi = \psi_{\text{PP}} + \psi_{\text{T}}, \quad (54)$$

where the coefficients of the 3.5PN order expansion of the point-particle contribution  $\psi_{\text{PP}}(x)$  are given in [32] and the tidal term,  $\psi_{\text{T}}$ , is calculated up to 1PN (relative) order in [2, 3, 9], by assuming a constant Love number. It reads

$$\psi_{\text{T}} = \psi_{\text{T}}^{\text{N}} + \psi_{\text{T}}^{\text{1PN}}, \quad (55)$$

with

$$\psi_{\text{T}}^{\text{N}}(f) = -\frac{3x^{5/2}}{128\nu m^5} \bar{\lambda}_2 \left[ \frac{24}{\chi_2} (1 + 11\chi_1) \right] + 1 \leftrightarrow 2, \quad (56)$$

$$\psi_{\text{T}}^{\text{1PN}}(f) = -\frac{3x^{5/2}}{128\nu m^5} \bar{\lambda}_2 \left[ \frac{5}{28\chi_2} (3179 - 919\chi_2 - 228\chi_2^2 + 260\chi_2^3) x \right] + 1 \leftrightarrow 2. \quad (57)$$

We may now use the Love function we introduced in Sec. III as an “upgrade” of the concept of Love number and determine new tidal contributions to the GW signal emitted by an inspiralling binary. Its  $r$ -dependency in Eq. (38) may be cast into a dependency on the PN dimensionless variable  $x$  by using the PN expansion of  $m/r$  in terms of  $x$  [33]. This way one has

$$k_2(x) = \bar{k}_2 [1 + \alpha x] + \mathcal{O}(x^2), \quad (58)$$

and consequently

$$\lambda(x) = \bar{\lambda} [1 + \alpha x] + \mathcal{O}(x^2), \quad (59)$$

where the coefficient  $\alpha$  is determined by means of our dynamical simulations. The expanded  $\lambda_A(x)$ ’s may now

replace the  $\bar{\lambda}_A$ ’s in the PN expanded energy  $\mathcal{E}(x)$  and GW flux  $\mathcal{L}_{\text{GW}}(x)$ , Eqs. (50) and (51) respectively. Notice that since the tidal correction to the binding energy and gravitational flux are known up to the 1PN order, Eq.(58) was truncated at  $\mathcal{O}(m/r) = \mathcal{O}(x)$ . We remark that the GW flux depends on the time derivatives of the quadrupole tensor of the system [9] and, therefore, the replacement  $\bar{\lambda}_A \rightarrow \lambda_A(x)$  in Eqns. (50) and (51) neglects terms arising from time derivatives of  $\lambda_A(x)$ . Such terms, however, being proportional to the velocities of the compact objects, are of a PN order higher than the order of the expansion in Eq.(57), and may be safely neglected. The replacement  $\bar{\lambda}_A \rightarrow \lambda_A(x)$  yields the following correction to the Fourier phase of the gravitational waveform given in Eq. (54):

$$\delta\psi_{\text{T}}(f) = -\frac{3x^{5/2}}{128\nu m^5} \bar{\lambda}_2 \left[ \frac{30}{7} \left( 2 + 27 \frac{\chi_1}{\chi_2} \right) \alpha_2 x \right] + 1 \leftrightarrow 2, \quad (60)$$

where  $\alpha_A$  are the coefficients appearing in Eq. (58) associated to the  $A - th$  body and  $\bar{\lambda}_A$  are determined from Eq.(52). Eq. (54) then becomes

$$\psi = \psi_{\text{PP}} + \psi_{\text{T}}^{\text{N}} + \psi_{\text{T}}^{\text{1PN}} + \delta\psi_{\text{T}}. \quad (61)$$

We remark that the term  $\psi_{\text{T}}^{\text{1PN}}$  and our correction  $\delta\psi_{\text{T}}$  have different origin. The former, obtained independently in [9] and in [41, 42], is the next-to-leading order tidal correction to the Fourier phase and was derived under the adiabatic approximation  $Q_{ij} = \bar{\lambda} C_{ij}$  (or, equivalently, assuming that the contribution of “electric” type quadrupole deformations to the action is  $\Delta S \sim \bar{\lambda} C_{ij} C_{ij}$ ); the latter is the result of a dynamical evolution in which we monitor the variation of the ratio between the quadrupole and tidal tensor during the inspiral (which we find to be the same, within  $\lesssim 1\%$ , for all components  $ij$ ); this variation is encoded in the parameter  $\alpha$  appearing in Eq. (59). Thus, these terms (both increasing as  $r$  decreases) simply add linearly.

In Fig. 2 we compare the different tidal contributions to the GW Fourier phase: the leading order term  $\psi_{\text{T}}^{\text{N}}$  (solid black line); the next-to-leading order  $\psi_{\text{T}} = \psi_{\text{T}}^{\text{N}} + \psi_{\text{T}}^{\text{1PN}}$  (dotted blue line); the total tidal contribution including our correction  $\psi_{\text{T}} + \delta\psi_{\text{T}}$ , (dashed-dotted red line). As discussed above, for consistency reasons our approach only allows us to include  $1/r$  ( $\sim x$ ) terms in the gravitational waveform, therefore we truncate our expansion at order  $\mathcal{O}(x)$ .

For each model the phases are shown in the range  $[10 \text{ Hz}, f_{\text{cut}}]$ , where  $f_{\text{cut}} = 2f_{\text{cut}}^{\text{orb}}$  (see Table I). Fig. 2 shows that:

- The dephasing due to the NS tidal deformation is significantly larger than one radian only for NS-NS binaries. For BH-NS binaries,  $\psi_{\text{T}} \lesssim 1$  rad and therefore, as previously established in [6], it is unlikely that second generation detectors such as Advanced LIGO/Virgo will detect tidal deformation effects in GWs emitted by mixed binaries. Only

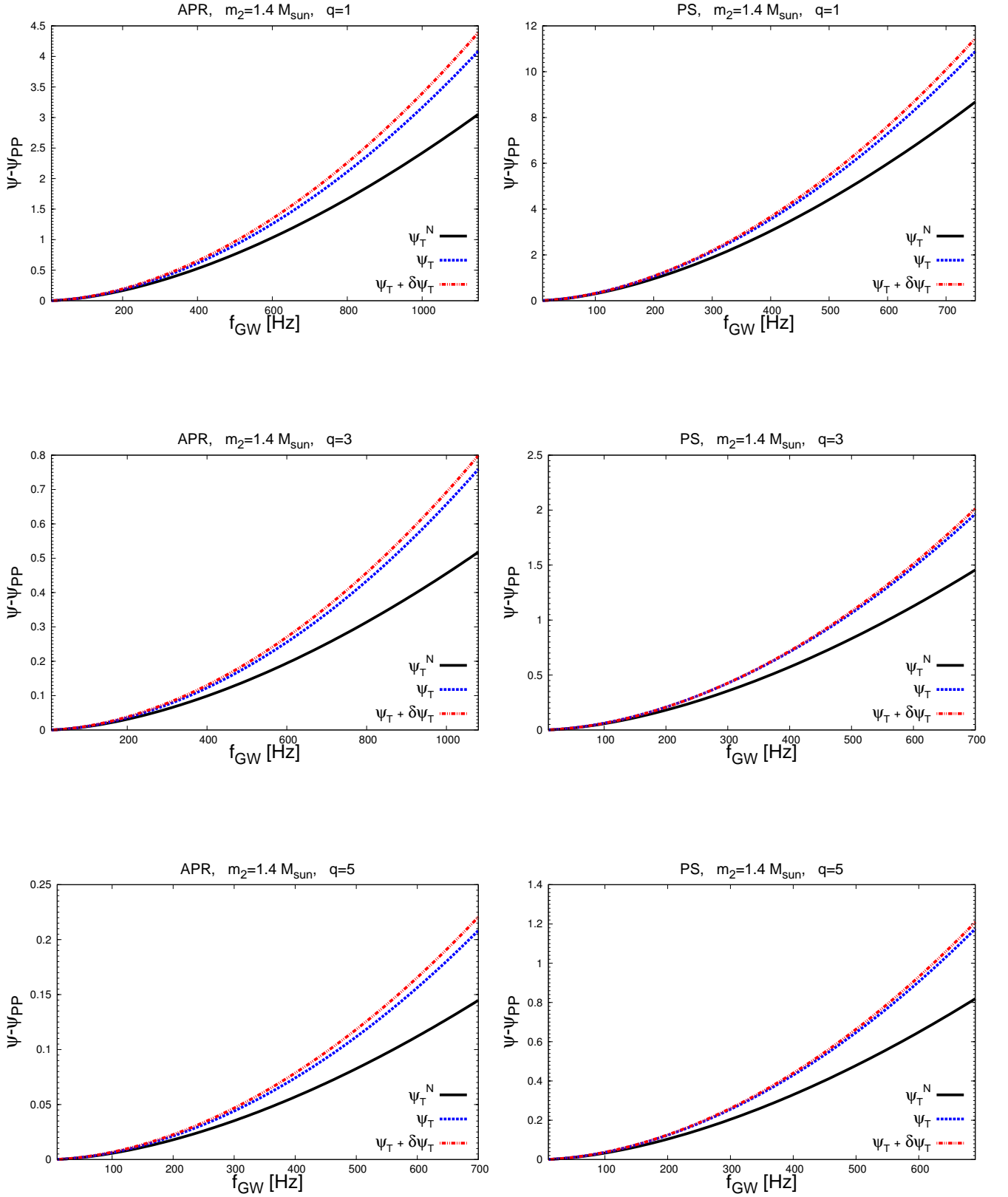


FIG. 2. (Color online) Tidal contribution to the Fourier phase of the gravitational wave signal, for  $m_2 = 1.4 M_\odot$ , the APR/PS EOS (left/right panels), and, from top to bottom,  $q = 1, 3$ , and  $5$ . Different curves show: the leading order term  $\psi_T^N$  (solid black line); the next-to-leading order contribution  $\psi_T = \psi_T^N + \psi_T^{1PN}$  (dotted blue line); the total tidal contribution including our correction  $\psi_T + \delta\psi_T$ , (dashed-dotted, red line). For each model the phases are shown in the GW frequency range  $[10 \text{ Hz}, f_{\text{cut}}]$ , where  $f_{\text{cut}} = 2f_{\text{cut}}^{\text{orb}}, f_{\text{cut}}^{\text{orb}}$  being the orbital frequencies given in Table I.

third generation detectors like the Einstein Telescope (ET) [43], which could detect signals with very large signal-to-noise ratio, would be able to reveal the tidal contribution in BH-NS binary coalescences.

- Looking at systems with  $q = 1$ , i.e., NS-NS binaries, the tidal signal is larger for stiffer EOS, or equivalently less compact NSs, and for lower values of the NS mass, confirming previous results [3, 42].
- The correction derived in this paper,  $\delta\psi_T$ , affects the GW phase only marginally for the binaries we consider. Indeed, the two curves describing  $\psi_T$  and  $\psi_T + \delta\psi_T$  nearly coincide.

Similar conclusions hold when we choose  $m_2 = 1.2M_\odot$ .

We remark that in our approach we determine the gravitational waveform up to the frequency  $f_{\text{cut}}$ , corresponding to the onset of the mass-shedding, which (in our PNA approach [16]) occurs when the NS fills its Roche lobe. As shown in Table I, we find values of  $f_{\text{cut}}$  between  $\sim 700$  and  $\sim 1150$  Hz. These values are larger than the cutoff frequency assumed in [3] ( $f_{\text{cut}} = 450\text{Hz}$ ), but more conservative than the values employed in [42], which correspond to the configuration in which the surfaces of the two bodies touch. As discussed in [3], the main reason behind the  $f_{\text{cut}} = 450\text{Hz}$  choice is that the next-to-leading order (1PN) corrections to the tidal phase, which we include, were neglected. On the other hand, the large values for  $f_{\text{cut}}$  used in [42] (see also [11]) correspond to the configuration in which the surfaces of the two bodies touch. We think that ending the integration when the NS fills its Roche lobe is a safer choice.

## V. WAVEFORM COMPARISONS

We now examine the dephasings discussed in the previous section in terms of GW detection. In order to do so, we calculate *overlaps* and *fitting factors* [28, 44] between point-particle waveforms, which we treat as our templates, and “real” signals, i.e. waveforms in which we include tidal effects to the best of our knowledge by means of Eq. (61). Our templates and signals thus have the form

$$\tilde{h}_{\text{PP}} = \mathcal{A}e^{i\psi_{\text{PP}}} \quad (62)$$

$$\tilde{h}_{\text{T},\delta} = \mathcal{A}e^{i(\psi_{\text{PP}} + \psi_{\text{T}}^{\text{N}} + \psi_{\text{T}}^{\text{1PN}} + \delta\psi_{\text{T}})}, \quad (63)$$

where  $\mathcal{A}$  denotes the GW amplitude and  $\psi_{\text{T}}^{\text{N}}$ ,  $\psi_{\text{T}}^{\text{1PN}}$ , and  $\delta\psi_{\text{T}}$  are the tidal contributions to the Fourier phase given in Eqs. (56), (57), and (60), respectively.

Given two signals  $h_1$  and  $h_2$ , their noise-weighted inner product is

$$\langle h_1 | h_2 \rangle \equiv 4\Re \int_{f_{\text{start}}}^{f_{\text{cut}}} df \frac{\tilde{h}_1(f) \tilde{h}_2^*(f)}{S_{\text{n}}(f)}, \quad (64)$$

where  $S_{\text{n}}(f)$  is the power spectral density of a given detector, the lower integration bound  $f_{\text{start}}$  depends on the detector one is examining, and for the upper bound  $f_{\text{cut}}$  we use twice the orbital frequency  $f_{\text{cut}}^{\text{orb}}$  discussed in the previous section. More specifically, we consider second and third generation detectors, such as Advanced Virgo/LIGO, and the Einstein Telescope, setting  $f_{\text{start}}$  to 20 Hz and 10 Hz, respectively, and follow [45] for  $S_{\text{n}}(f)$ . The inner product allows us to define the overlap between two signals, that is, their normalized inner product, maximized over time and phase shifts:

$$\mathcal{O}[h_1, h_2] \equiv \max_{\{\tau, \varphi\}} \frac{\langle h_1 | h_2 \rangle}{\sqrt{\langle h_1 | h_1 \rangle \langle h_2 | h_2 \rangle}}, \quad (65)$$

where  $\tau$  and  $\varphi$  are the time and phase offsets between the two waveforms. This quantity is useful, for example, when describing in quantitative terms the effectiveness of a waveform model in detecting a physical waveform. Furthermore by maximising  $\mathcal{O}[h_1, h_2]$  over the intrinsic, physical parameters of, say,  $h_1$ , one obtains the fitting factor. In our case, the point-particle waveform templates,  $\tilde{h}_{\text{PP}}$ , depend on the binary total mass and symmetric mass ratio, so that we denote the fitting factor with  $\mathcal{FF}(m, \nu)$ .

As discussed in [28], when calculating the number of missed events in a search performed with a discrete template bank, one must take into account the template bank spacing and the fitting factor  $\mathcal{FF}(m, \nu)$  between the template GW model and the real signal model. In the case of LIGO/Virgo template banks, this may be done by subtracting a maximum mismatch of 0.03 to the fitting factors we calculate: this yields the effective fitting factors  $\mathcal{EFF}(m, \nu) = \mathcal{FF}(m, \nu) - 0.03$  which must then be used to determine the fraction of missed events  $1 - \mathcal{EFF}(m, \nu)^3$ . [28] additionally discusses a criterion for template waveform accuracy:  $1 - \mathcal{FF}(m, \nu)$  must be smaller than 0.005, so that  $1 - \mathcal{EFF}(m, \nu) < 0.035$  for LIGO/Virgo.

Our results may be summarized as follows:

- We find that the lowest overlaps occur in the case of low mass ratios as already noted in [6]; this happens for two reasons, in general: because low total masses and mass ratios enhance the dephasing in Eqs. (56), (57) and (60) and because  $f_{\text{cut}}$  is higher for lower mass systems, thus allowing the phase difference originating from tidal distortions to accumulate over a broader frequency range. Furthermore, in the  $q = 1$  case the phase difference originates from the distortion of two NSs instead of a single one.
- For BH-NS binaries, the  $\mathcal{O}[h_{\text{PP}}, h_{\text{T},\delta}]$  overlaps are  $\gtrsim 0.997$  for second generation detectors and  $\gtrsim 0.995$  for the Einstein Telescope, as already found in [6]. This means that (1) point-particle templates are within the needed waveform accuracy, since  $1 - \mathcal{FF} \leq 1 - \mathcal{O} \leq 0.005$ , and that (2) the

total number of missed events including the effect of template bank spacing, is  $1 - \mathcal{EF}\mathcal{F}(m, \nu)^3 \leq 1 - (\mathcal{O} - 0.03)^3 \lesssim 10\%$ .

- For second generation detectors and NS-NS binaries, we find that, depending on the EOS, the overlap  $\mathcal{O}[h_{PP}, h_{T,\delta}]$  varies within the range  $[0.963, 0.997]$  for  $m_2 = 1.2M_\odot$  and within  $[0.982, 0.999]$  for  $m_2 = 1.4M_\odot$ ; the lower limits correspond to larger deformabilities, i.e. to the stiffer, PS EOS. For third generation detectors, the intervals are, instead,  $[0.943, 0.992]$  and  $[0.969, 0.997]$ .
- By computing the fitting factors for NS binaries with the PS EOS, we obtain  $\mathcal{FF}(m, \nu) = 0.991$  for  $m_2 = 1.2M_\odot$  and  $\mathcal{FF}(m, \nu) = 0.996$  for  $m_2 = 1.4M_\odot$ , in the case of second generation detectors. For third generation detectors, one has, instead,  $\mathcal{FF}(m, \nu) = 0.985$  for  $m_2 = 1.2M_\odot$  and  $\mathcal{FF}(m, \nu) = 0.992$  for  $m_2 = 1.4M_\odot$ .
- In the case of Advanced LIGO/Virgo and of a particularly stiff EOS for matter in the NS interior, the total number of missed events corresponding to the above fitting factors,  $1 - \mathcal{EF}\mathcal{F}(m, \nu)^3$ , may thus be as high as 11% for low mass NS binaries, whereas it would roughly be 10% for a canonical  $m = 2.8M_\odot$  equal mass NS binary. The Einstein Telescope, on the other hand, would miss up to  $\sim 13\%$  low mass NS-NS inspirals and up to 11% canonical NS inspirals. Our results are summarized in Tables II, III.
- If the EOS of NS matter is very stiff, point-particle templates of binary NS inspirals would not meet the required accuracy for Advanced Virgo/LIGO in the case of a low total mass, since the fitting factor we obtain yields  $1 - \mathcal{FF}(m, \nu) > 0.005$  [28]. The same is true for equal mass NS inspirals and the Einstein Telescope, on the high stiffness end of possible EOSs. As previously mentioned, the PS EOS is an extreme case of stiff EOS. Nevertheless, one should consider this worst (in terms of missed events and waveform template accuracy) case scenario and establish if, and eventually how, we may remedy; this is important also because a lot of interesting physics is associated with low mass NS binary mergers, e.g. [46, 47]. If one imagines to use templates  $\tilde{h}_{T,PN}$  that include tidal corrections up to (relative) 1PN order in the Fourier phase by means of the *Love Number*, i.e.

$$\tilde{h}_{T,1PN} = \mathcal{A}e^{i\psi_{PP} + i\psi_T^N + i\psi_T^{1PN}} \quad (66)$$

all overlaps  $\mathcal{O}[h_{T,1PN}, h_{T,\delta}]$  would differ from unity by less than a part in one-thousand, both for second and third generation detectors. To the best of our knowledge in the modelling of the real signal, the inclusion of Love Number dependent tidal terms in GW templates would therefore greatly help in constraining the NS EOS in post-processing analysis,

confirming the result of [42]. Building gravitational waveforms within the adiabatic approximation (i.e., including  $\psi_T^N$  and  $\psi_T^{1PN}$ ) is thus very reliable.

- Let us now suppose that the EOS of NS matter is stiff and that an  $m = 2.4M_\odot$  equal mass binary NS inspirals close enough to Earth. The detection of its gravitational radiation by a second generation detector with an imaginarily infinitesimally spaced template bank would hit a point-particle template with total mass  $m = 2.446M_\odot$  and symmetric mass ratio  $\nu = 0.242$ , since these are the values that maximise the overlap  $\mathcal{O}[h_{PP}, h_{T,\delta}]$ : this means that tidal effects contribute with a 2% error to the total mass measurement and with a 3% error on the symmetric mass ratio measurement. In the case of an  $m = 2.8M_\odot$  equal mass inspiral, the tidal contributions to the errors on the total mass and the symmetric mass ratio measurements would be 1% and 2%, respectively. The same values hold for third generation detectors.

EOS	$m(M_\odot)$	$\mathcal{O}[h_{PP}, h_{T,\delta}]$	$\mathcal{FF}(m, \nu)$	# missed
APR	2.4	0.997	1.000	0%
	2.8	0.999	1.000	0%
PS	2.4	0.963	0.991	11%
	2.8	0.982	0.996	9.8%

TABLE II. We report the values of overlaps  $\mathcal{O}[h_{PP}, h_{T,\delta}]$  and fitting factors  $\mathcal{FF}(m, \nu)$  between point-particle templates and waveforms in which we include tidal effects evaluated as in Eq. (61). We also show the total number of missing events. All values refer to NS-NS systems and second generation detectors AdVirgo/LIGO.

EOS	$m(M_\odot)$	$\mathcal{O}[h_{PP}, h_{T,\delta}]$	$\mathcal{FF}(m, \nu)$	# missed
APR	2.4	0.992	1.000	0%
	2.8	0.997	1.000	0%
PS	2.4	0.943	0.985	13%
	2.8	0.969	0.992	11%

TABLE III. The same quantites of Table II, but for third generation detector ET.

## VI. CONCLUDING REMARKS

In this paper we improve the PNA model recently developed in [16], by computing the tidal tensor of a binary system up to 2 PN order. Using this approach, we study the dynamical evolution of NS deformations in compact binary inspirals, finding a number of interesting results.

We find that the ratio between the quadrupole tensor  $q_{ij}$  and the tidal tensor  $c_{ij}$  increases during the last stages of the inspiral, and we show that the Love number has to

be considered as the asymptotic value of this ratio for sufficiently large orbital separation. This increase, however, only marginally affects the phase of the emitted signal, thus assessing the validity of the adiabatic approximation when modeling the gravitational wave signal.

We provide a semi-analytical expression of the Love number, in terms of the scalar quadrupole moment and of the integral of pressure over the stellar volume, both computed for the star at isolation, i.e. for a spherically symmetric configuration (Eq. (49)). This expression provides a physical insight on the Love number and a formulation alternative to that given in [12], only in terms of quantities which refer to the structure of the star in its spherical equilibrium configuration.

In addition, we estimate the reliability of point par-

ticle templates with respect to a “real” signal modeled by means of our approach, finding that such templates marginally fail to meet the standard accuracy requirements ( $1 - \mathcal{FF}(m, \nu) < 0.005$ ) for NS-NS inspirals with very stiff equation of state.

## ACKNOWLEDGEMENTS

We thank L. Rezzolla, A. Nagar, and D. Bini for useful discussions. This work was partially supported by CompStar, a research networking program of the European Science Foundation. F.P. was supported in part by the DFG grant SFB/Transregio 7.

- 
- [1] <http://www.ego-gw.it>; <http://www.ligo.caltech.edu>.
  - [2] E.E. Flanagan, T. Hinderer, Phys. Rev. **D77**, 021502 (2008).
  - [3] T. Hinderer, B.D. Lackey, R.N. Lang, J.S. Read, Phys. Rev. **D81**, 123016 (2010).
  - [4] T. Damour, A. Nagar, Phys. Rev. D **80**, 084035 (2009).
  - [5] T. Damour, A. Nagar, Phys. Rev. **D81**, 084016 (2010).
  - [6] F. Pannarale, L. Rezzolla, F. Ohme and J. S. Read, Phys. Rev. D **84**, 104017 (2011).
  - [7] J.S. Read, C. Markakis, M. Shibata, K. Uryu, J.D.E. Creighton, J.L. Friedman, Phys. Rev. D **79**, 124033 (2009).
  - [8] L. Baiotti, T. Damour, B. Giacomazzo, A. Nagar, L. Rezzolla, Phys. Rev. Lett. **105**, 261101 (2010).
  - [9] J. Vines, E.E. Flanagan, T. Hinderer, Phys. Rev. **D83**, 084051 (2011).
  - [10] B.D. Lackey, K. Kyutoku, M. Shibata, P.R. Brady, J.L. Friedman, Phys. Rev. D **85**, 044061 (2012).
  - [11] S. Bernuzzi, A. Nagar, M. Thierfelder, B. Bruegmann, arXiv:1205.3403.
  - [12] T. Hinderer, Astrophys. J. **677**, 1216 (2008); *ibid.*, **697**, 964 (2009).
  - [13] T. Binnington, E. Poisson, Phys. Rev. D **80**, 084018 (2009).
  - [14] K.S. Thorne, A. Campolattaro, Astrop. J., **149**, 591 (1967).
  - [15] D. Lai, Mon. Not. Roy. Astron. Soc. **270**, 611 (1994).
  - [16] V. Ferrari, L. Gualtieri, A. Maselli, Phys. Rev. **D85**, 044045 (2012).
  - [17] L. Blanchet, A. Buonanno, and G. Faye, Phys. Rev. D, **74**, 104034 (2006).
  - [18] L. Blanchet, A. Buonanno, and G. Faye, , Phys. Rev. D, **84**, 064041 (2011).
  - [19] L. Blanchet, Living Rev. Relativity, **9**, 4 (2006).
  - [20] B. Carter, J.P. Luminet, Mon. Not. R. Astron. Soc. **212**, 23 (1985).
  - [21] J.P. Luminet, J.A. Marck, Mon. Not. R. Astron. Soc. **212**, 57 (1985).
  - [22] P. Wiggins, D. Lai, Astrophys. J. **532**, 530 (2000).
  - [23] C. Casavieri, V. Ferrari, A. Stavridis, Mon. Not. R. Astron. Soc. **365**, 929 (2006).
  - [24] V. Ferrari, L. Gualtieri, F. Pannarale, Class. Quant. Grav. **26**, 125004 (2009).
  - [25] V. Ferrari, L. Gualtieri, F. Pannarale, Phys. Rev. **D81**, 064026 (2010).
  - [26] B.S. Sathyaprakash, S.V. Dhurandhar, Phys. Rev. **D44**, 3819 (1991).
  - [27] C. Cutler, E.E. Flanagan, Phys. Rev. **D49**, 2658 (1994).
  - [28] L. Lindblom, B.J. Owen, and D.A. Brown, Phys. Rev. **D78**, 124020 (2008).
  - [29] B. Carter, J.P. Luminet, A& A **121**, 97 (1983).
  - [30] L. Blanchet, G. Faye, and B. Ponsot, Phys. Rev. **D58**, 124002 (1998).
  - [31] G. Faye, L. Blanchet, and A. Buonanno, Phys. Rev. **D74**, 104033 (2006).
  - [32] L. Santamaria et al., Phys. Rev. **D82**, 064016 (2010).
  - [33] Marc Favata, Phys. Rev. D **83**, 024027 (2011).
  - [34] J.-A. Marck, Proc. Roy. Soc. Lond. **Q385**, 431, (1983).
  - [35] T. Damour, M. Soffel, C. Xu, Phys. Rev. **D45**, 1017 (1992).
  - [36] T. Fukushima, Cel. Mech. and Dynamical Astron. **44**, 61 (1988).
  - [37] D. Lai, F.A. Rasio, S.L. Shapiro, Astrophys. J. **437**, 742 (1994).
  - [38] A. Akmal, V.R. Pandharipande, D.G. Ravenhall, Phys. Rev. **C58**, 1804 (1998).
  - [39] V.R. Pandharipande, R.A. Smith, Nucl. Phys. **A237**, 507 (1975).
  - [40] T. Damour, B.R. Iyer, B. S. Sathyaprakash, Phys. Rev. **D63**, 044023 (2001); [Erratum-*ibid.* **D 72**, 029902 (2005)].
  - [41] D. Bini, T. Damour, G. Faye, Phys. Rev. **D 85**, 124034 (2012).
  - [42] T. Damour, A. Nagar, L. Villain, Phys. Rev. **D 85**, 123007 (2012).
  - [43] M. Punturo, et al., Classical Quantum Gravity, **27**, 084007 (2010).
  - [44] B.J. Owen, Phys. Rev. **D53**, 6749 (1996).
  - [45] B.S. Sathyaprakash, and B.F. Schutz, Living Rev. Relativ., **12**, 2 (2009).
  - [46] M. Shibata, Y. Suwa, K. Kiuchi, and K. Ioka, Astrophys. J. Lett., **734**, L36 (2011).
  - [47] A. Bauswein, H.-T. Janka, K. Hebeler, A. Schwenk, arXiv:1204.1888 (2012).